ISSN 1063-7710, Acoustical Physics, 2013, Vol. 59, No. 1, pp. 6–15. © Pleiades Publishing, Ltd., 2013.
Original Russian Text © E.V. Glushkov, N.V. Glushkova, O.A. Godin, 2013, published in Akusticheskii Zhurnal, 2013, Vol. 59, No. 1, pp. 8–18.

CLASSICAL PROBLEMS OF LINEAR ACOUSTICS AND WAVE THEORY

The Effect of Anomalous Transparency of the Water–Air Interface for a Volumetric Sound Source

E. V. Glushkov[a], N. V. Glushkova[a], and O. A. Godin[b]

[a] *Kuban State University, ul. Stavropol'skaya 149, Krasnodar, 350040 Russia*
e-mail: evg@math.kubsu.ru

[b] *University of Colorado and NOAA/Earth System Research Laboratory, Boulder, CO 80505 USA*

Received March 10, 2012

Abstract—Anomalous transparency consists in the passage at certain frequencies of the majority of a source's radiated energy through an interface, which usually gives strong reflection. Earlier, this effect was established for low-frequency point sources located in a fluid bounded by an air medium. In the case of volumetric sources, additional scattering of waves occurs between the interface of the media and the emitter surface; and the character of the manifestation of this effect is unclear. This work, using the solution to the integral equation corresponding to a boundary value problem, examines the emission of wave energy by spherical sources of different radius and its distribution between the energy flow passing through the water–air interface into the upper half-space and the energy flow going to infinity in the lower half-space. It has been established that the size of the source has virtually no effect on the energy distribution in the low-frequency range, i.e., on the anomalous transparency effect. We also analyze how the relative dimensions of spherical sources affect the energy characteristics in the mid- and high-frequency range.

Keywords: spherical emitter, integral equation, wave energy, anomalous transparency
DOI: 10.1134/S106377101206005X

INTRODUCTION

Due to the strong contrast in the densities of air and water, the interface of these media is a virtually ideal reflector of hydroacoustic signals. However, for point sources operating in the low-frequency range, the anomalous transparency effect has been revealed [1, 2], when a significant (and if the frequency tends toward zero, overwhelming) part of the wave energy emitted by the source into a fluid is captured by energy flows traveling toward its surface, it passes through the boundary, and it exits into the air medium. The effect takes place at the interface of homogeneous and inhomogeneous fluids and gases [2–4], as well as of a solid and a gas [5, 6]. A characteristic feature of point sources is their transparency, i.e., the absence of repeat scattering for reflected waves arriving at it from media interfaces and other obstacles. In the case of emitters of finite size, multiple reflections occurs between their surfaces and the media interface, which affects sound energy radiation and transfer.

To confirm the possibility of and analyze the features of manifestation of the anomalous transparency effect for real sound sources, this work considers a boundary value problem on the steady-state harmonic oscillations of a spherical emitter located in the lower half-space of a dual-layer water–air space. A rigorous account of the interaction between reflected waves and the source leads to an integral equation with respect to the unknown density distribution of wave potential q on its surface. Its numerical solution is constructed by discretizing integral representations with derivation of the contribution from the singular component of the kernel in explicit form. The excited wave field is thereby approximated by superposing the field of elementary monopole sources located on the surface of the sphere. Their amplitudes are determined from a linear algebraic system, to which the integral equation is reduced as a result of discretization. This approach is known as the wave superposition method [7].

Analysis of the efficiency of various methods conducted using a test problem of sound emission from a spherical source [8] has shown that among comparative approaches, this method ensures the highest accuracy with the lowest numerical expenditures. However, it does not yield a solution in the vicinity of a discrete set of frequencies—points of the spectrum of the integral operator—that coincide with the discrete spectrum of the Dirichlet problem for the internal volume of the emitter. This is because, in the general case, the field emitted by the source should consist of monopole and dipole fields and at the indicated eigenfrequencies, the monopole fields alone become insufficient for satisfying the boundary conditions. One-valued solvability at points of the spectrum of the internal Dirichlet problem is achieved by using more complex formulations, such as the combined Helmholtz inte-

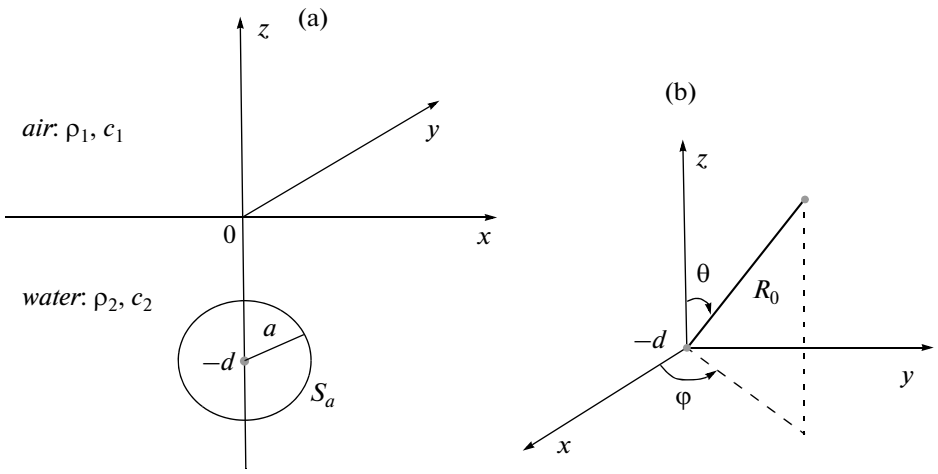

Fig. 1. Geometry of the problem (a) and local spherical coordinates (b).

gral equation formulation (CHIEF) [9]. On the other hand, the addition of dipole sources to the set of basis functions increases computational costs. In the case considered, the dimensionless frequencies of false resonances $\omega_n = n\pi d/a$, $n = 1, 2, \ldots$ are far to the right of the low-frequency range of interest to us and violations of numerical stability are observed only in a very small vicinity of these frequencies. Therefore, here the use of the simpler wave superposition method is quite justified.

Since the fundamental solution to the Helmholtz equation (i.e., the field due to a point monopole), which is used in the classical approach as the kernel of the integral operator, does not satisfy the boundary conditions at the media interface, in the suggested mathematical model, we use the Green's function for the considered two-layer space on the whole. Each of the summands of the constructed wave field identically satisfies the boundary conditions at the water–air interface, and the total field of elementary sources also satisfies the conditions at the emitter surface. In this sense, this approach can be considered a variant of the layered elements method, the main idea of which is to use a set of elementary solutions as the basis, which automatically satisfy the boundary conditions at horizontal layer boundaries [10]. In contrast to [11], where in solving a related problem, a high-frequency asymptotics [12] of the Green's function was used, in this work, the Green's function is calculated exactly as an integral over plane waves.

Along with numerical analysis, an asymptotic analysis of the considered wave processes is conducted, which in the limiting case gives the same quantitative estimates. Here, the derivation and use of asymptotics of scattering of spherical waves by an obstacle are essential, since the amplitude of the reflected wave can change strongly at distances on the order of the obstacle size.

The analysis conducted using the mathematical model outlined above has shown that the effect of anomalous transparency is also retained for volumetric sources. Moreover, it turns out that in the low-frequency region, the power radiated by various types of spherical sources and the distribution of emitted energy E between the energy E^+ departing into the air medium and the energy E^- remaining in the fluid depends weakly on their sizes. The results we obtain for higher frequencies are of independent interest.

FORMULATION OF THE PROBLEM AND GENERAL SOLUTION SCHEME

We consider steady-state vibration harmonics $\mathbf{u}(\mathbf{x})e^{-i\omega t}$, $\mathbf{x} = (x, y, z)$ of the acoustic medium, which consists of two half-spaces with different properties given by sound velocity c_n and density ρ_n, $n = 1, 2$. The vibration source is a spherical emitter of radius a located in the lower half-space ($n = 2$) at depth d (Fig. 1a). Velocity $v e^{-i\omega t}$ of its surface S_a : $R_0 = a$ displacement is assumed given:

$$v_R\big|_{\mathbf{x}\in S_a} = v. \tag{1}$$

Here, $R_0 = R_0(-d) = \sqrt{x^2 + y^2 + (z+d)^2}$; $v_R = (\mathbf{v}, \mathbf{n}_s)$ is the normal (radial) component of the velocity vector of fluid particle vibration $\mathbf{v} = -i\omega\mathbf{u}$; $\mathbf{n}_s = \{\cos\varphi\sin\theta, \sin\varphi\sin\theta, \cos\theta\}$ is the unit external normal to the surface S_a; harmonic multiplier $e^{-i\omega t}$ is omitted from this point on. Along with Cartesian coordinates (x, y, z), spherical coordinates (R_0, φ, θ) are also used (Fig. 1b). The two sets of coordinates are related by

$$\begin{aligned} x &= R_0\cos\varphi\sin\theta, \quad R_0 = |\mathbf{x} - \mathbf{x}_0|, \mathbf{x}_0 = (0,0,-d),\\ y &= R_0\sin\varphi\sin\theta, \qquad 0 \le \varphi \le 2\pi,\\ z &= R_0\cos\theta - d, \qquad 0 \le \theta \le \pi. \end{aligned}$$

The displacement and velocity vector fields are expressed in terms of the scalar pressure field $p(\mathbf{x})$:

$$\mathbf{u} = \frac{1}{\omega^2\rho}\nabla p \text{ and } \mathbf{v} = \frac{1}{i\omega\rho}\nabla p, \quad (2)$$

which in each of the half-spaces satisfies the Helmholtz equation

$$\Delta p + \kappa_n^2 p = 0 \quad (3)$$

with the wavenumber $\kappa_n = \omega/c_n$, $n = 1, 2$ ($n = 1$ for $z > 0$ and $n = 2$ for $z < 0$). It is assumed that pressure field p and the vertical component of the displacement vector $u_z = \frac{1}{\omega^2\rho}\frac{\partial p}{\partial z}$ are continuous at the media interface $z = 0$:

$$[p] = 0, \quad [u_z] = 0. \quad (4)$$

Square brackets denote the jump in the corresponding function at the surface $z = 0$: $[f] = \lim_{\varepsilon\to 0}(f(z-\varepsilon) - f(z+\varepsilon))$. In addition, to ensure one-valued solvability of boundary problem (1)–(4), the radiation conditions at infinity, which follow from the limiting absorption principle, need to be fulfilled [13].

The integral representation of the general solution to the given problem is constructed using the Green's function $g(\mathbf{x}, \boldsymbol{\xi})$, which is derived as the fundamental solution corresponding to a point source $\delta(\mathbf{x} - \boldsymbol{\xi})$ (δ is the Dirac delta function) located at point $\boldsymbol{\xi} = (\xi, \eta, \zeta)$ of the lower half-space:

$$\begin{aligned} \Delta g + \kappa_1^2 g &= 0, \quad z > 0, \\ \Delta g + \kappa_2^2 g &= \delta(\mathbf{x} - \boldsymbol{\xi}), \quad z < 0, \end{aligned} \quad (5)$$

$$[g] = 0, \quad \left[\frac{1}{\rho}\frac{\partial g}{\partial z}\right] = 0, \quad z = 0. \quad (6)$$

Function g can be represented as the sum of the classical fundamental solution to the Helmholtz equation:

$$g_0(\mathbf{x} - \boldsymbol{\xi}) = g_0(R) = -\frac{1}{4\pi}e^{i\kappa_2 R}/R, \; R = |\mathbf{x} - \boldsymbol{\xi}|, \quad (7)$$

i.e., a particular solution to the second of Eqs. (5) describing the field of a point source in an infinite space, and the corrective term $g_{sc}(\mathbf{x}, \boldsymbol{\xi})$ occurring due to the interaction of the field g_0 with the media interface $z = 0$:

$$g(\mathbf{x}, \boldsymbol{\xi}) = \begin{cases} g_{sc}(\mathbf{x}, \boldsymbol{\xi}), & z \geq 0, \\ g_0(\mathbf{x} - \boldsymbol{\xi}) + g_{sc}(\mathbf{x}, \boldsymbol{\xi}), & z \leq 0. \end{cases} \quad (8)$$

The reflected ($z < 0$) and refracted ($z > 0$) field g_{sc} is constructed in explicit form using Fourier transform over the horizontal coordinates x, y. As a result

$$g(\mathbf{x}, \boldsymbol{\xi}) = \frac{1}{(2\pi)^2}\int\!\!\int_{\Gamma_1\Gamma_2} G(\alpha, z, \zeta)e^{-i[\alpha_1(x-\xi)+\alpha_2(y-\eta)]}d\alpha_1 d\alpha_2, \quad (9)$$

$$G = \begin{cases} G_{sc} = -\dfrac{1}{2\sigma_2}b_1(\alpha)e^{\sigma_2\zeta}e^{-\sigma_1 z}, & z \geq 0, \\ G_0 + G_{sc} = -\dfrac{1}{2\sigma_2}[e^{-\sigma_2|z-\zeta|} + b_2(\alpha)e^{\sigma_2(z+\zeta)}], & z \leq 0, \end{cases}$$

$$b_1(\alpha) = \frac{2\rho_1\sigma_2}{\rho_1\sigma_2 + \rho_2\sigma_1}, \quad b_2(\alpha) = \frac{\rho_1\sigma_2 - \rho_2\sigma_1}{\rho_1\sigma_2 + \rho_2\sigma_1},$$

$$\sigma_n = \sqrt{\alpha^2 - \kappa_n^2}, \quad \mathrm{Re}\,\sigma_n \geq 0, \quad \mathrm{Im}\,\sigma_n \leq 0, \quad n = 1, 2.$$

Quantities b_1 and b_2 have the meaning of transmission and reflection coefficients for plane waves with a horizontal wavevector (α_1, α_2, 0) [12]. The integration contours Γ_1, Γ_2 go along the real axes in the complex planes α_1, α_2, deviating from them around branch points $\alpha = \pm\kappa_n$, $n = 1, 2$ in accordance with the limiting absorption principle.

For any point $\boldsymbol{\xi}$ located within sphere S_a, function $g(\mathbf{x}, \boldsymbol{\xi})$ satisfies Helmholtz Eqs. (3) and the boundary conditions at the media interface (4). Any superposition of such functions has the same property, as well as does the integral

$$p(\mathbf{x}) = \int\!\!\int_{S_a^-} g(\mathbf{x}, \boldsymbol{\xi})q(\boldsymbol{\xi})d\boldsymbol{\xi}, \quad (10)$$

taken over the surface of a sphere S_a^- of smaller radius $\bar{a} = a - \varepsilon$ ($\varepsilon > 0$, $\varepsilon/a \ll 1$). This formulation yields the sought solution to original problem (1)–(4) if the unknown density of potential $q(\boldsymbol{\xi})$ is chosen such that the radial component of the velocity vector

$$\mathbf{v}(\mathbf{x}) = \frac{1}{i\omega\rho_2}\int\!\!\int_{S_a^-} \nabla g(\mathbf{x}, \boldsymbol{\xi})q(\boldsymbol{\xi})d\boldsymbol{\xi}, \quad (11)$$

also satisfies the conditions at the surface of sphere (1). Substitution of formulation (11) into condition (1) leads to the integral equation with respect to the unknown q,

$$\mathcal{H}q \equiv \int\!\!\int_{S_a^-} k(\mathbf{x}, \boldsymbol{\xi})q(\boldsymbol{\xi})d\boldsymbol{\xi} = f(\mathbf{x}), \quad \mathbf{x} \in S_a \quad (12)$$

with the kernel

$$k(\mathbf{x}, \boldsymbol{\xi}) = (\nabla g(\mathbf{x}, \boldsymbol{\xi}), \mathbf{n}_s) = \frac{\partial g(\mathbf{x}, \boldsymbol{\xi})}{\partial \mathbf{n}_s}$$

and the given right-hand side $f(\mathbf{x}) = i\omega\rho_2 v(\mathbf{x})$. In accordance with representation of g as the sum $g_0 + g_{sc}$, the kernel is also split into two summands: $k = k_0 + k_{sc}$, where k_{sc} is an infinitely smooth function and k_0 has a singularity:

$$k_0(\mathbf{x}, \boldsymbol{\xi}) = \frac{\partial g_0}{\partial \mathbf{n}_s} \sim -\frac{1}{4\pi}\frac{\partial}{\partial \mathbf{n}_s}\left(\frac{1}{R}\right) \text{ at } R \to 0.$$

In the limit at $\varepsilon \to 0$, i.e., when the radius of the internal sphere $\bar{a}$ tends to a, a point of singularity $\mathbf{x} = \boldsymbol{\xi}$ appears at the integration surface and the surface integral in Eq. (12) is understood as an integral in the sense of the principal value plus the contribution of the integral over the internal infinitely small half-sphere S_ε: $|\mathbf{x} - \boldsymbol{\xi}| = R = \varepsilon$ obviating the point of singularity $\mathbf{x}$. As $\varepsilon \to 0$, this integral reduces to a Gaussian integral

yielding the value of the solid angle at which this half-sphere is visible from point **x**:

$$I = \lim_{\varepsilon\to 0}\int\int_{S_\varepsilon}\frac{\partial}{\partial \mathbf{n}_s}\left(\frac{1}{R}\right)dS = \int_0^{\pi}\int_0^{\pi}\sin\psi\, d\chi\, d\psi = -2\pi.$$

Equation (12) thereby takes the classical form of an equation of the second kind with the contribution of the singular kernel component revealed in explicit form:

$$\frac{1}{2}q(\mathbf{x}) + \text{v.p.}\int\int_{S_a} k(\mathbf{x},\xi)q(\xi)d\xi = f(\mathbf{x}), \quad \mathbf{x}\in S_a. \qquad (13)$$

It is noteworthy that as ξ approaches **x** along surface S_a, the singularity of the kernel in fact becomes removable because vector $\mathbf{i}_R = \nabla R = (\mathbf{x}-\xi)/R$ entering into

$$k_0 = (\nabla g_0, \mathbf{n}_s) = (i\kappa_2 - 1/R)(\mathbf{i}_R, \mathbf{n}_s)g_0,$$

in the limit becomes orthogonal to normal vector $\mathbf{n}_s$: $(\mathbf{i}_R, \mathbf{n}_s)\to 0$ at $\xi\to\mathbf{x}$. Therefore, numerical integration in the vicinity of point of singularity **x** in local polar coordinates ($d\xi = RdRd\varphi$) does not require reduction of the grid step at $R\to 0$.

The solution to integral equation (13) is sought in the form of an expansion over the system of certain basis function q_j specified on the integration surface S_a:

$$q(\xi)\approx q_N(\xi) = \sum_{j=1}^{N} t_j q_j(\xi). \qquad (14)$$

The unknown expansion coefficients t_j grouped into vector $\mathbf{t} = (t_1, t_2, ..., t_N)^T$ are determined from the linear algebraic system

$$A\mathbf{t} = \mathbf{f}, \qquad (15)$$
$$A = [a_{ij}]_{i,j=1}^{N}, \quad \mathbf{f} = (f_1, f_2, ..., f_N)^T,$$

to which Eq. (13) reduces after substitution in it of q of form (14) and subsequent discretization according to the Galerkin scheme or the collocation method.

The simplest to implement is the selection as basis q_j of functions equal to unity in the elementary cells S_j in which surface S_a is split during discretization and to zero in its remaining part. In this case, when the collocation method is used, the elements of matrix A and the right-hand side of f of system (15) have the following form:

$$a_{ij} = \frac{1}{2}\delta_{ij} + \text{v.p.}\int\int_{S_i} k(\mathbf{x}_i,\xi)d\xi, \quad f_i = f(\mathbf{x}_i).$$

Here δ_{ij} is the Kronecker symbol and $\mathbf{x}_i\in S_i$ are the colocation points. With increasing N, the convergence $t_j\to q(\xi_j)$, $\xi_j\in S_a$ takes place; i.e., expansion (14) gives a piecewise continuous approximation of the sought density of potential q on the surface S_a.

In the case of axial symmetry, where function $v = v(\theta)$ does not depend on angle variable φ in the source definition (1), solution q also depends only on one polar angle ψ of the spherical system of coordinates (a, χ, ψ): $\xi = a\cos\chi\sin\psi$, $\eta = a\sin\chi\sin\psi$, $\zeta = a\cos\psi - d$, $0\le\chi<2\pi$, $0\le\psi\le\pi$, which determines the location of point ξ on S_a. In these coordinates the integral over χ from the kernel k is evaluated in explicit form; i.e., the integral operator of Eq. 12 becomes one-fold. For expansion q, it suffices then to specify a system of basis functions $q_j(\psi)$ on the segment of polar angles $0\le\psi\le\pi$, having fixed the colocation points on the meridian $R_0 = a$, $\varphi = 0$, $0\le\theta\le\pi$. Along with the piecewise continuous approximation, here expansion in terms of hat functions was also used,

$$q_j(\psi) = s((\psi-\psi_j)/h), \quad s(x) = \begin{cases}1-|x|, & |x|<1,\\ 0, & |x|>1,\end{cases}$$
$$\psi_j = (j-1/2)h, \quad h = \pi/N, \quad j = 1,2,...,N,$$

giving a piecewise linear approximation.

After finding coefficients t_j, the wave field characteristics can be calculated at an arbitrary point of space **x** (outside of S_a) using superposition of the fields of elementary sources q_j:

$$p(\mathbf{x})\approx\sum_j t_j p_j(\mathbf{x}), \quad \mathbf{u}(\mathbf{x})\approx\sum_j t_j\mathbf{u}_j(\mathbf{x}),$$
$$p_j = \int\int_{S_j} g(\mathbf{x},\xi)q_j(\xi)d\xi, \quad \mathbf{u}_j = \frac{1}{\omega^2\rho}\nabla p_j. \qquad (16)$$

The time-averaged over the period of vibrations $T = 2\pi/\omega$ energy flux E transferred in the harmonic wave field through a certain surface S is determined using integration of the normal component e_n of the energy flux density vector **e** over this surface [14]:

$$E = \int\int_S e_n dS, \quad e_n = (\mathbf{e},\mathbf{n}) = \frac{\omega}{2}\text{Im}(\tau_n, \mathbf{u}). \qquad (17)$$

Here **n** is the normal to surface S at the current integration point ξ, and τ_n is the stress vector in the elementary area with normal **n**. In the fluid, $\tau_n = -p\mathbf{n}$ and, as a consequence, $e_n = \text{Im}\left(\frac{\partial p}{\partial\mathbf{n}}p^*\right)/(2\omega\rho)$, $\frac{\partial p}{\partial\mathbf{n}} = (\nabla p, \mathbf{n})$; the asterisk denotes complex conjugation.

The permeability of the media interface for the wave energy flux is estimated using the transparency coefficient [1]

$$\mu = 10\log_{10}(E^+/E)\,(\text{dB}), \qquad (18)$$

in which E^+ is the amount of energy passing into the upper half-space and E is the total amount of energy radiated by the source into the medium. To calculate E^+ in formulation (17), the surface $z = 0$ should be

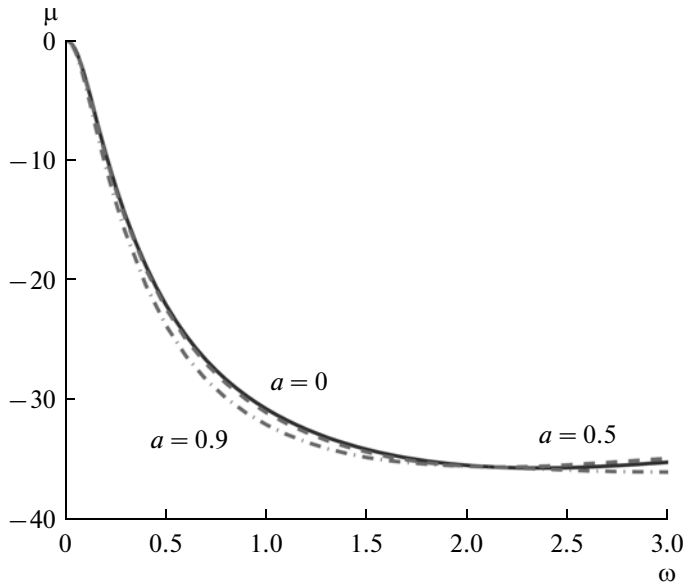

Fig. 2. Frequency dependences of transparency coefficient μ illustrating the weak influence of the relative size of a spherical emitter on the given characteristic.

taken as S, and surface S_a should be taken for E. However, due to the energy conservation law, $E = E_b$, where E_b is the total energy flux through any spherical surface S_b of radius $b > a$ concentric with S_a. In addition, owing to the absence of the outflow of energy to infinity in the horizontal direction, $E^+ = E_z$, where E_z is the energy flux through any horizontal plane $z =$ const located higher than the source ($z > a - d$). Analogously, the amount of energy E^- departing from the source into the lower half-space is equal to E_z at any $z < -a - d$. Numerical verification of the energy conservation law, as well as the energy balance $E = E_b = E^+ + E^-$, was used to control the reliability of the results.

ENERGY DISTRIBUTION OF A SPHERICAL SOURCE

Analysis of how the relative size of the source a/d affects the distribution of emitted energy E between fluxes E^+ and E^- and, as a result, transparency coefficient μ has led to a somewhat unexpected result. Calculations have shown that despite rigorous allowance in the considered model for multiple reflections between the media interface and the emitter's surface, with increasing a/d the E^+/E ratio (and therefore μ) remains almost completely the same as that obtained earlier [1, 2] for a point source! This conclusion is illustrated by the dependences of μ, E and $E^\pm$ on dimensionless frequency ω for a point monopole and spherical sources with a relative radius of $a/d = 0.1$, 0.5, and 0.9 (Figs. 2, 3).

All of the results are given in dimensionless form, in which the depth of the center of the source d, the velocity of sound in a fluid c_2, and its density ρ_2 are taken as unity. As well, the dimensionless circular frequency $\omega = \kappa_2 d = 2\pi f d/c_2$, where f is the dimensional frequency in Hertz, and the dimensionless time-averaged power of the source $E = \hat{E}\rho_2 c_2^3 d^2$, where $\hat{E}$ is the dimensional power in Watts. The dimensionless parameters of the medium $c_1 = 0.222$, $\rho_1 = 0.0013$, and $c_2 = 1$, $\rho_2 = 1$ correspond to the dimensional parameters $c_1 = 330$ m/s, $\rho_1 = 1.3$ kg/m^3, and $c_2 = 1485$ m/s, $\rho_2 = 1000$ kg/m^3 for air and water, respectively.

We considered three types of axially symmetric sources: an M source (monopole) with a uniform velocity distribution v_R over S_a in condition (1) ($v = v_0 = \text{const}$), as well as V and H sources with dominance, respectively, of the vertical or horizontal velocity components $\mathbf{v}$ on S_a:

$$V: v(\theta) = 6\left|\cos^5\theta\right| v_0, \quad H: v(\theta) = \frac{32}{5\pi}\sin^5\theta\, v_0,$$
$$0 \le \theta \le \pi.$$

The coefficients here were selected so that in all three cases, the volume velocity of sources $\hat{v}$ were the same:

$$\hat{v} = \frac{1}{4\pi a^2}\int\int_{S_a} v\,dS = \frac{1}{2}\int_0^\pi v(\theta)\sin\theta\,d\theta = v_0.$$

In addition, for comparison of the results, constant v_0 was chosen such that at low frequencies, the spherical M source was energetically equivalent to a point δ source, i.e., so that at $\omega \to 0$, their energy E_0 radiated into an infinite space coincided. For a point source with a field g_0 of form (7), $E_0 = 1/(8\pi c_2\rho_2)$, and for a spherical M source,

$$E_0 = \frac{2\pi a^4 \rho_2 c_2 \omega^2}{c_2^2 + a^2\omega^2}|v_0|^2,$$

Therefore, the required equivalence is ensured at $v_0 = 1/(4\pi\rho_2\omega a^2)$, and not only at $\omega \to 0$, but also at $a \to 0$.

Axial symmetry simplifies the analysis; in particular, surface integrals (17) are reduced to single ones:

$$E = 2\pi a^2\int_0^\pi e_n(\theta)\sin\theta\,d\theta, \quad e_n = \frac{1}{2}\mathrm{Re}[p(\theta)v^*(\theta))], \tag{19}$$
$$p(\theta) = p|_{R_0=a},$$
$$E^+ = \frac{1}{8\pi\omega\rho_2}$$
$$\times\left[\int_0^{\kappa_2}\frac{1-|b_2(\alpha)|^2}{2\sqrt{\kappa_2^2-\alpha^2}}|Q|^2\,\alpha\,d\alpha + \int_{\kappa_2}^{\kappa_1}\frac{\mathrm{Im}\,b_2(\alpha)}{\sqrt{\alpha^2-\kappa_2^2}}|Q|^2\,\alpha\,d\alpha\right],$$

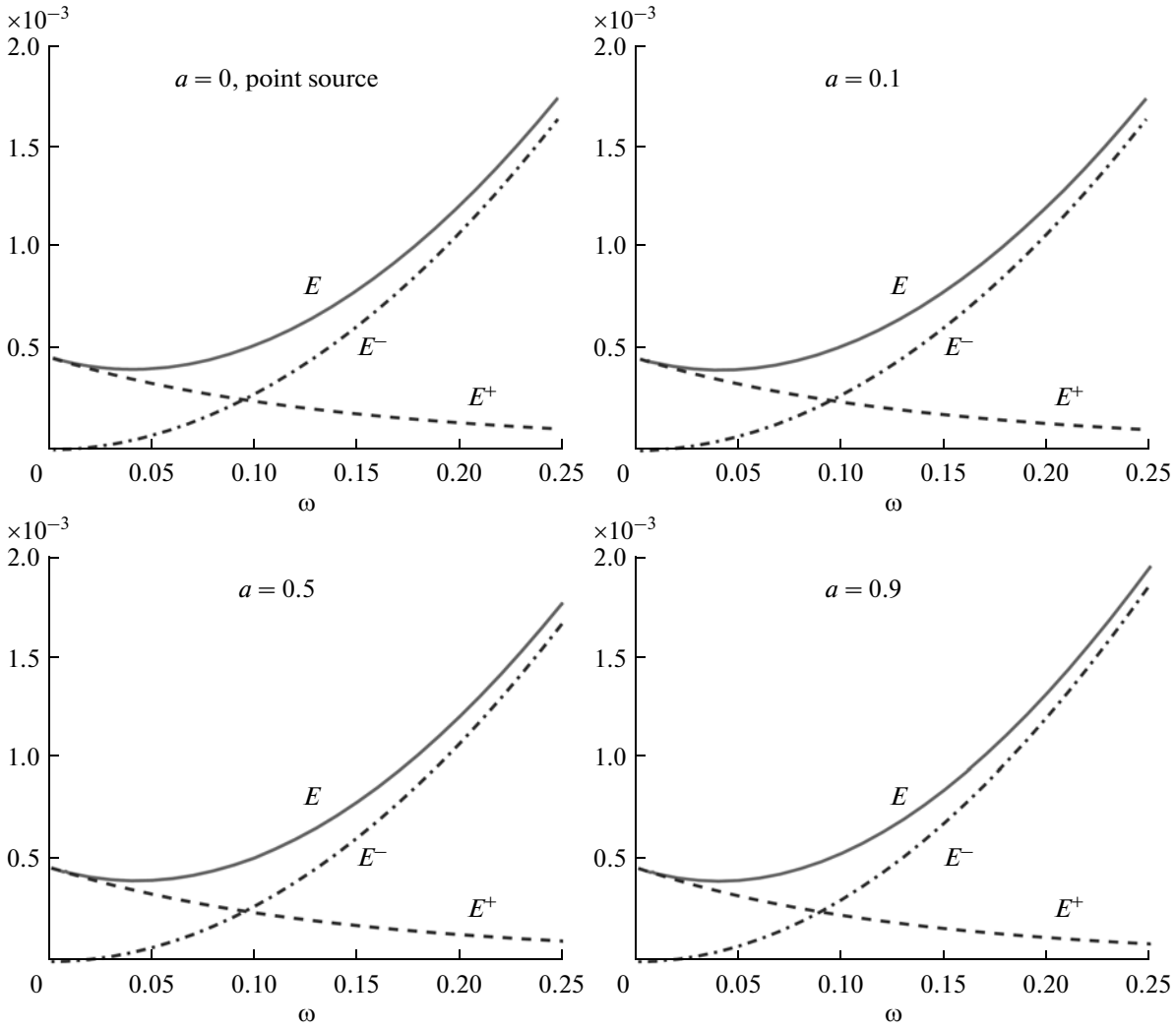

Fig. 3. Low-frequency distribution of the total radiated power E between energy fluxes E^+ and E^- for point ($a = 0$) and spherical M sources of different radius a.

$$E^- = \frac{1}{16\pi\omega\rho_2} \times \int_0^{\kappa_2} -\frac{(|Q_1|^2 + |b_2(\alpha)Q_2|^2 + 2\mathrm{Re}[b_2(\alpha)Q_1^*Q_2])}{\sqrt{\kappa_2^2 - \alpha^2}}\alpha d\alpha,$$

$$Q(\alpha) = 2\pi a^2 \int_0^{\pi} \hat{q}(\psi) e^{\sigma_2\zeta} d\psi,$$

$$Q_{1,2}(\alpha) = 2\pi a^2 \int_0^{\pi} \hat{q}(\psi) e^{\sigma_2(z\mp\zeta)} d\psi,$$

$\hat{q}(\psi) = q(\psi)J_0(\alpha a\sin\psi)\sin\psi$, $\zeta = a\cos\psi - d$, J_0 is the Bessel function.

In Fig. 2, the solid line shows the dependence of transparency coefficient μ on $\omega = \kappa_2 d$ for a point source; this dependence coincides with that obtained earlier [1, 2]. The dashed line and dash-dotted lines show the μ values for a medium ($a = 0.5$) and a large ($a = 0.9$) spherical M sources. In all three cases, $\mu \to 0$ at $\omega \to 0$; i.e., the boundary $z = 0$ becomes anomalously transparent. Moreover, these plots show that transparency μ hardly depends at all on the relative size of the M source in the entire range of frequencies ω considered. Analysis of the dependences $\mu(\omega)$ calculated for V and H sources lead to similar conclusions.

The dependences $E^{\pm}(\omega)$ in Fig. 3 show that in the low-frequency range, the size of the source has practically no effect on not only the E^+/E^- ratio, but also on the amount of emitted energy E^+ and E^- separately. Moreover, dependences like those in Fig. 3 are also obtained for V and H sources. It is interesting that point ω at which E^- becomes equal to E^+ in all cases is approximately the same: $\omega \approx 0.1$. A more detailed analysis shows that its value still depends on a, but only in the third digit. So, e.g., for M sources (Fig. 3), $E^+ =$

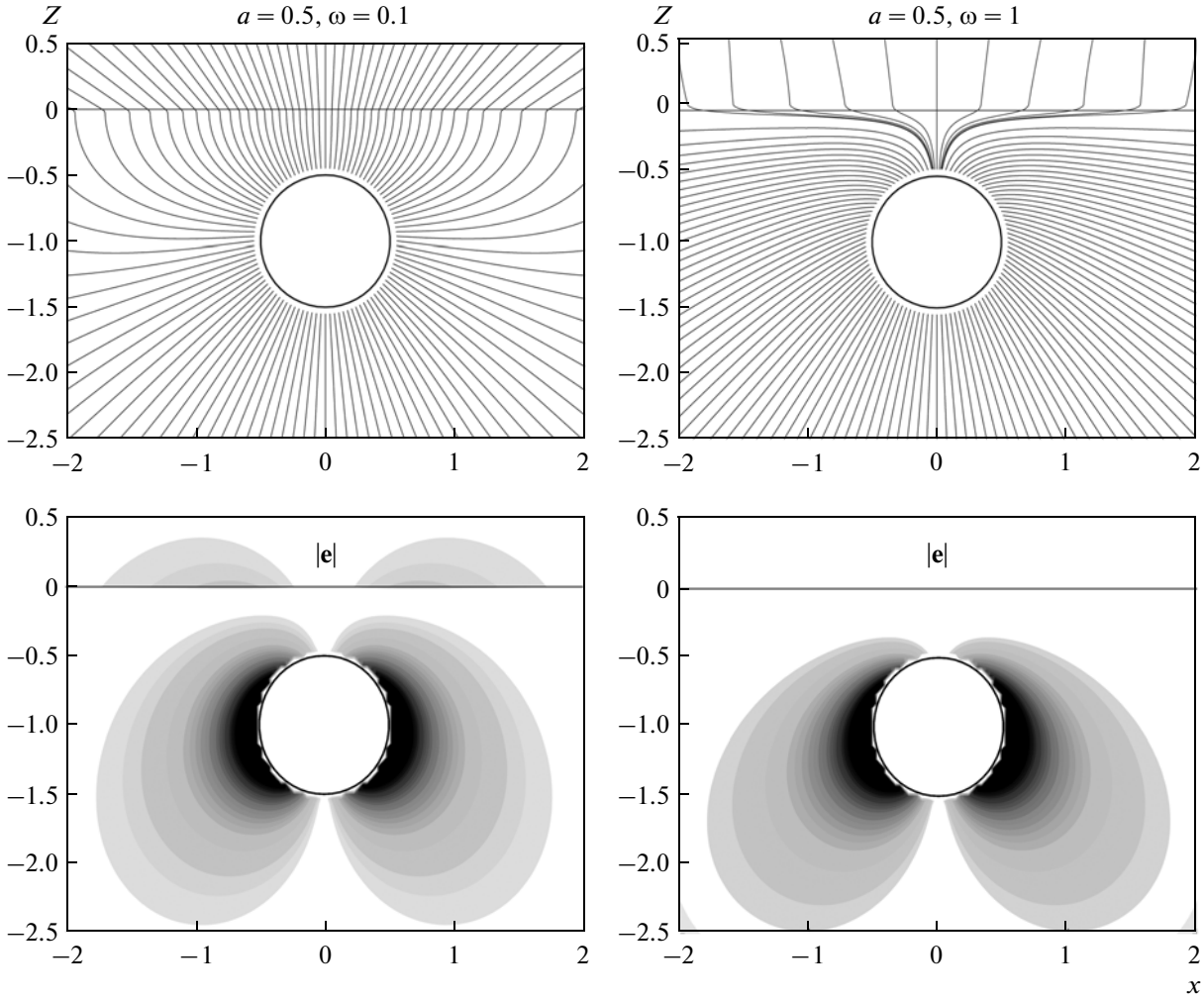

Fig. 4. Energy streamlines (top) and energy flux density $|\mathbf{e}(x, z)|$ (bottom) for an M source of radius $a = 0.5$ and low ($\omega = 0.1$, left) and medium ($\omega = 1$, right) frequencies.

E^- at $\omega = 0.097$, 0.097, 0.095, and 0.089 for $a = 0$, 0.1, 0.5, and 0.9, respectively.

The energy streamlines generated by the vector field **e(x)** give a visual picture of the averaged over the period of oscillations wave energy transfer from the source to infinity (at any point **x**, vector **e** is tangential to the streamline passing through this point) (Fig. 4). The surface of the source S_a is split into two parts S_a^+: $0 \le \theta < \theta_0$ and S_a^-: $\theta_0 \le \theta \le \pi$. The streamlines that originate from surface S_a^+, intersect the boundary $z = 0$, indicating the path of transfer of energy E^+ from the fluid into the air. At low frequencies, when $E^+ > E^-$, S_a^+ takes up a large part of surface S_a ($\theta_0 \to \pi$ at $\omega \to 0$), but with an increase in ω, polar angle θ_0, determining the boundary between S_a^+ and S_a^-, decreases monotonically, and in accordance with the behavior of the $E^\pm$ curves (Fig. 3), intersects the equator ($\theta_0 = \pi/2$) at $\omega \approx 0.1$ (Fig. 4, left). At $\omega = 1$ (Fig. 4, right), angle θ_0 is already comparatively small and energy goes into the air only from a narrow vicinity of the pole of the sphere $\theta = 0$. On the whole, the pattern of streamlines and character of changes in it with frequency are the same as for a point source [15].

In Fig. 4, the corresponding energy flux density distribution $|\mathbf{e}(x, z)|$ is shown below the energy streamlines. Characteristic features of it are an increased energy flux density emitted to the side (dark areas along the side surface of the source) and its nearly zero flux density going from near-polar regions (vertical light stripes above and below the source). The low energy flux density from the near-polar region along with a decrease in area S_a^+ leads to a rapid drop in the fraction of E^+ with increasing ω.

The radiated energy E can also be represented as the sum $E = E_0 + E_{sc}$, in which E_{sc} gives a correction to energy E_0, which occurs owing to wave reflection. At low frequencies, this correction is negative and

$E_{sc} \approx -E_0$ at $\omega \to 0$; as a result, $E \ll E_0$ (Fig. 5). With increasing ω, the contribution of E_{sc} decreases. For the chosen dependence v_0 on ω, which has a power-law decrease, the energy E_0 of a spherical M source also has a power-law decrease: $E_0 \sim c_2/(8\pi a^2 \rho_2 \omega^2)$ at $\omega \to \infty$. Therefore, the $E(\omega)$ curves in Fig. 5 reach a maximum in a certain mid-frequency range, then, at high frequencies, tend to zero. At the same time, for a point source $E_0 = \text{const}$; i.e., this selection of v_0 provides energy equivalent of volumetric and point sources only in the low-frequency region, which expands with decreasing a.

The frequency range in Fig. 5 contains false resonances at $a = 0.5$ ($\omega_1 = 6.28$) and $a = 0.9$ ($\omega_1 = 3.49$, $\omega_2 = 6.98$). Their presence is manifested in the form of relatively small dips on the corresponding $E(\omega)$ curves in the vicinity of these frequencies. With increasing approximation accuracy owing to an increased number of basis functions N (the plots in Fig. 5 is are calculated using $N = 40$), the zones of numerical instability narrow rapidly and the spurious dips become invisible.

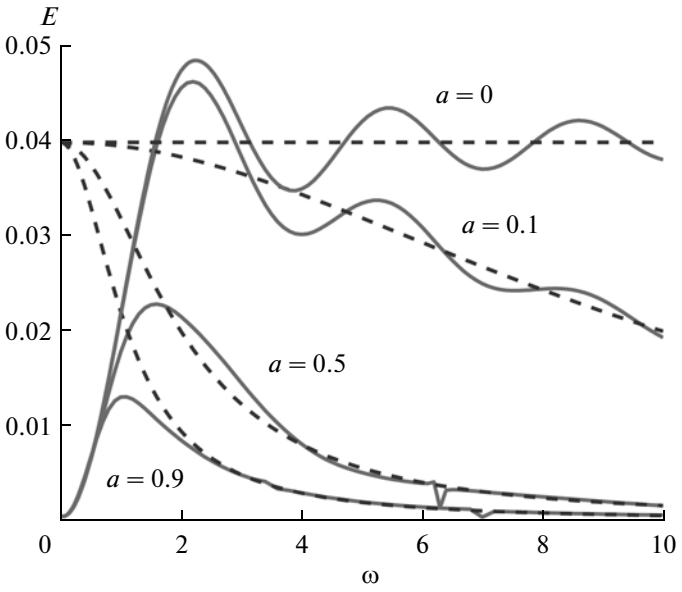

Fig. 5. Frequency dependence of total radiated power E of a point ($a = 0$) and three spherical M sources (solid lines) and the power E_0 radiated by these sources into a homogeneous space (dashed line).

SOUND EMISSION BY A SOURCE OF FINITE SIZE AS A SCATTERING THEORY PROBLEM

To clarify the reasons behind the insensitivity of the interface transparency to the properties of a low-frequency source, it is expedient to study the emitted sound field analytically. In a homogeneous fluid, the field of an M source coincides at $R_0 > a$ with the field of a point monopole source. When an incident spherical wave created by the M source is incident on the boundary, the waves that are transmitted into the air and reflected into water are the same as in the case of a point source; however, a reflected wave is then scattered on the surface of the finite source. During interaction with the boundary, a singly scattered wave, similarly to the initial spherical wave, again generates a transmitted and a reflected wave, and the reflected wave is again scattered on the surface of the source, etc.

Since on the surface of the considered sound source the value of the normal velocity is assumed to be fixed, the normal velocity in the superposition of a wave incident on the source and scattered by the source is equal to zero at $R_0 = a$. This means that the source scatters sound like a rigid sphere of radius a. In the single scattering approximation, ignoring small corrections on the order of ρ_1/ρ_2, the wave incident on the source becomes a spherical wave originating from the point (0, 0, d) located in the upper half-space. Thus, here arises the problem on scattering of a spherical wave on a rigid sphere.

Note that the standard theory of Rayleigh scattering [16] is inapplicable in this case, since pressure in an incident wave significantly changes within the limits of the scatterer when the relative size of the source a/d is on the order of unity. An elementary solution to the problem on scattering of a spherical wave on a small rigid sphere has the following form [17, 18]:

$$p_{sc} = -\frac{\kappa_2^2 a^3}{24\pi d R_0} e^{i\kappa_2(R_0+2d)} + \frac{1-2ik_2 d}{4\pi a} e^{2i\kappa_2 d} \int_0^{a^2/2d} z_0 \frac{\partial}{\partial z_0}\left[\frac{\exp(i\kappa_2 R_0(z_0))}{R_0(z_0)}\right] dz_0. \quad (20)$$

Here, $R_0(z_0) = \sqrt{x^2 + y^2 + (z - z_0)^2}$ and it is taken into account that a wave incident on a spherical scatterer p_{in} has the same form (7) as for $-g_0$ but with $R = R_0(d)$.

A scattered wave p_{sc} coincides with the sound field generated by imaginary sources: a monopole at the center of the sphere and vertical dipoles distributed along the segment $\{x = 0, y = 0, -d < z < -d + a^2/2d\}$ within the scatterer. Therefore, in the single scattering approximation, an M source is equivalent to a set of point sound-transparent sources.

From formula (20) it follows that although the scattered field near the scatterer is not small in comparison to an incident wave, relative perturbations of the power flux, averaged over the wave period, through any plane not intersecting the scatterer are small in terms of the $\kappa_2 a$ parameter at any values $a/d \le 1$. This result admits a simple physical interpretation: strong perturbations of the sound field near a small, in comparison to the wavelength, scatterer result from inhomogeneous waves with wavenumbers on the order of

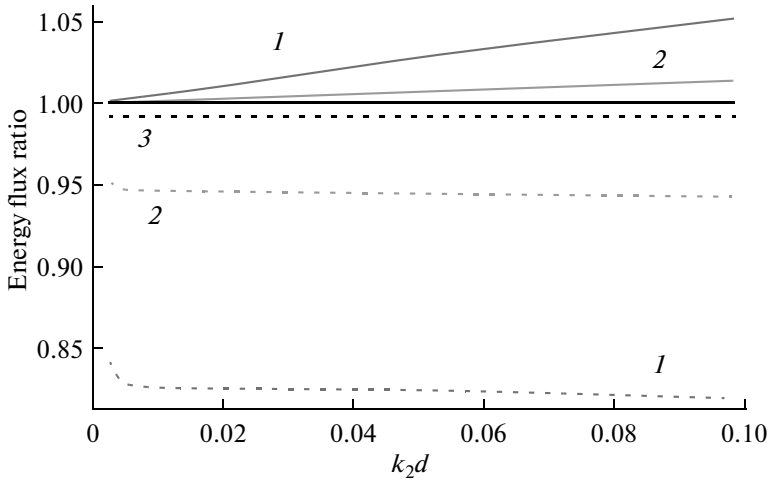

Fig. 6. Frequency dependence of radiation by a source with finite dimensions. Power fluxes E^+ (solid lines) and E^- (dashed lines) generated by M sources with relatives size of $a/d = 0.9$ (*1*), 0.6 (*2*), and 0.3 (*3*) are normalized to the corresponding power fluxes from equivalent point sources.

$1/a$; these waves attenuate rapidly with distance from the receiver and do not emit sound.

The solution to the problem of sound emission by an arbitrary sound-transparent source in the presence of an interface is expressed in terms of the plane-wave spectrum of the field created by the source in an infinite medium [3]. Using Eqs. (9) and (20), for the plane-wave spectra above and below the source, we obtain

$$S_{1,2}(\alpha) = 1 + \frac{\exp(2i\kappa_2 d)a^3}{24d^2}[4\kappa_2^2 d + (\pm 3i - 2\kappa_2 d \pm 4\kappa_2 d)\sqrt{\kappa_2^2 - \alpha^2}(1 + O(\kappa_2^2 a^2))]. \quad (21)$$

The upper and lower signs here refer to S_1 at $z < -a - d$ and to S_2 at $a - d < z < 0$, respectively. For simplicity, it is assumed that a is small not only in comparison to $1/\kappa_2$ but also to $1/\kappa_1$. We emphasize that the deviations of S_1 and S_2 from unity at $\alpha < \kappa_1$ as a result of the finite size of the source remain small at any $a/d \le 1$. Therefore, at $\alpha < \kappa_1 \ll a^{-1}$, allowance for multiple scattering leads only to the appearance in S_1 and S_2 of terms of higher order in the small parameter $\kappa_2 a$.

In terms of S_1 and S_2, acoustic power fluxes radiated to infinity in the air and water are given by Eqs. (11) and (12) in [3] (cf. (19)):

$$E^+ = \frac{E_0}{\kappa_2}\left[\int_0^{\kappa_2}\frac{1 - |b_2(\alpha)|^2}{2\sqrt{\kappa_2^2 - \alpha^2}}\left|S_2^2\right|\alpha d\alpha + \int_{\kappa_2}^{\kappa_1}\frac{\mathrm{Im}\, b_2(\alpha)}{\sqrt{\alpha^2 - \kappa_2^2}}\left|S_2^2\right|\alpha d\alpha\right], \quad (22)$$

$$E^- = \frac{E_0}{2\kappa_2}\int_0^{\kappa_2}\left|S_1 + b_2(\alpha)S_2\exp(2id\sqrt{\kappa_2^2 - \alpha^2})\right|^2\frac{\alpha d\alpha}{\sqrt{\kappa_2^2 - \alpha^2}}.$$

According to Eqs. (21) and (22), the effect of the finite dimensions of an M source on sound emission manifests itself in the first order of $\kappa_2 a$ at $\kappa_2 d \ll 1$ and only in the second order at $\kappa_2 d \sim 1$. When values of E_0 and $\kappa_2 d$ are fixed, the effect of the source's size increases as the third power of the a/d ratio. The effect of finite source dimensions on sound radiation into air and water is illustrated in Figs. 6 and 7, which are obtained using Eqs. (21) and (22). These asymptotic results agree well with the results presented in Figs. 2, 3, and 5 obtained by solving integral equation (13) derived with a strict allowance for reflected waves interaction with the emitting sphere.

In the geometric acoustics approximation, perturbations of the acoustic energy flux due to scattering of a spherical wave on a localized obstacle is proportional to the solid angle at which it is visible from the center of the incident wave. At $a/d \to 1$, the source is visible from point $(0, 0, d)$ at an angle of $\pi(2 - \sqrt{3})$ sr, and significant (on the order of $O(1)$) perturbations of E^+ and E^- can be expected. As demonstrated above, for low-frequency sound, this does not occur owing to diffraction effects, and corrections remain small in terms of parameter $\kappa_2 a$, even despite the fact that the air–water boundary is located in the near zone of the source.

CONCLUSIONS

In this work, using spherical sound sources as an example, it has been shown that the effect of low-frequency anomalous transparency of the air–water interface established earlier for point sources also takes place in the case of sound sources with finite dimensions. As expected, for a sharp increase in boundary transparency and radiation of the majority of the wave energy into the air to occur, smallness of the linear dimensions of the source is necessary in comparison to the wavelength. On the contrary, despite expectations, for manifestation of the effect at

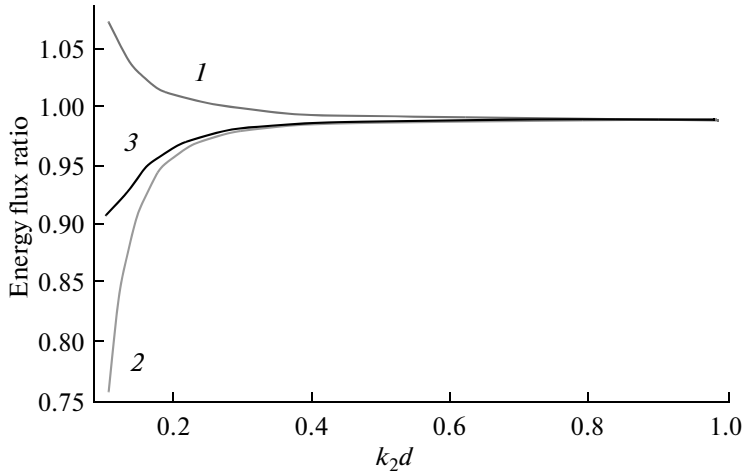

Fig. 7. Sound emission by a source with a small wave dimension at different distances to the water–air interface. The ratios of the power fluxes generated by an M source and by a point source that go to infinity in air (*1*) and water (*2*) and the ratio of the total radiated acoustic powers (*3*) are shown as functions of dimensionless depth $\kappa_2 d$ of the sources. The radius of the M source is $a = 0.1\kappa_2^{-1}$.

low frequencies, i.e., when the source depth is small compared to the wavelength, smallness of the source dimensions in comparison to its depth is not required. It has been found that, for sources with a fixed volume velocity and small wave dimensions, both the total acoustic power radiated in the two-layer medium and the ratio of wave energy fluxes into water and air are almost independent of the ratio of the source radius to its depth. This result stems from certain peculiarities of wave diffraction on objects with small wave dimensions. It sharply broadens the range of phenomena for which the theory predicts anomalous transparency of the water–air interface for low-frequency sound and significantly simplifies set-up of laboratory and full-scale experiments for verifying the theory.

ACKNOWLEDGMENTS

The work was carried out with financial support from the Russian Foundation for Basic Research (project no. 12-01-00320).

REFERENCES

1. O. A. Godin, Phys. Rev. Lett. **97**, 164301 (2006).
2. O. A. Godin, Akust. Zh. **53**, 353 (2007) [Acoust. Phys. **53**, 305 (2007)].
3. O. A. Godin, Contemp. Phys. **49**, 105 (2008).
4. M. Hornikx and R. Waxler, J. Comput. Acoust. **18**, 297 (2010).
5. R. S. Matoza, D. Fee, and M. A. Garcés, J. Geophys. Res. B **115**, B12312 (2010).
6. O. A. Godin, J. Acoust. Soc. Am. **129**, 45 (2011).
7. G. H. Koopman, L. Song, and J. B. Fahnline, J. Acoust. Soc. Am. **86**, 2433 (1989).
8. G. W. Benthien and H. A. Schenck, Comp. Struct. **65**, 295 (1997).
9. H. A. Schenck, J. Acoust. Soc. Am. **44**, 41 (1968).
10. E. V. Glushkov, N. V. Glushkova, A. A. Eremin, and V. V. Mikhas'kiv, Prikl. Mat. Mekh. **73**, 622 (2009).
11. M. Zampolli, A. Tesei, G. Canepa, and O. A. Godin, J. Acoust. Soc. Am. **123**, 4051 (2008).
12. L. M. Brekhovskikh and O. A. Godin, *Acoustics of Inhomogeneous Media*. Vol. 1: *Fundamentals of Sound Reflection and Propagation Theory* (Nauka, Moscow, 2007) 446 p. [in Russian].
13. A. G. Sveshnikov, Dokl. Akad. Nauk SSSR **80**, 345 (1951).
14. N. A. Umov, *Selected Papers* (Gostekhizdat, Moscow, 1950) [in Russian].
15. D. M. F. Chapman, J. Acoust. Soc. Am. **124**, 48 (2008).
16. M. A. Isakovich, *General Acoustics* (Nauka, Moscow, 1973) [in Russian].
17. O. A. Godin, J. Acoust. Soc. Am. **130**, EL135 (2011).
18. O. A. Godin, *Proc. Conf. OCEANS'11 MTS/IEEE Kona, Hawaii, 2011*, pp. 1–9.